https://doi.org/10.1590/jatm.v17.1373 ORIGINAL PAPER

Simulation and Measurement of Plume Characteristics of a Hall Thruster with 12.5 kW

Mingming Sun[1,*], Hai Geng[1], Chao Liu[1], Jun Gao[1], Pei Li[1], Shangmin Wang[1]

1. China Academy of Space Technology – Lanzhou Institute of Physics – Science and Technology on Vacuum Technology and Physics Laboratory – Lanzhou/Gansu – China.

*Corresponding author: smmhappy@163.com

ABSTRACT

To rapidly and cheaply obtain the plume characteristics of a 12.5 kW Hall thruster, a simulation model based on the fluid method is developed, and a plume measurement is conducted to verify and compare with the simulations. The results show that the discharge process will mainly occur in the upper part of the discharge channel, and the error between simulations and measurements of the magnetic field is less than 5%. The pressure in the discharge channel is the highest and the average pressure is about 0.12 Pa. In the plume diffusion region, the plasma density decays slightly along the axial direction and rapidly in the radial direction. Additionally, the plasma density and the electron temperature from the discharge channel outlet to the upper boundary of the plume region are in the range of 6.2×10^{16} to 5.2×10^{17} m^{-3} and 1.8 to 12.2 eV, respectively. In the plume measurement, a single Faraday probe is used to scan and measure the beam current, and the simulations are consistent with the experiments. The simulation model basically achieves the purpose of obtaining the plume characteristics with certain accuracy, low cost and rapidly.

Keywords: Hall thruster; Ion beams; Plasma discharges; Plasma diagnostics.

INTRODUCTION

Based on the advantages of lower cost and high reliability, Hall thrusters have been widely used in many space missions such as satellite orbit adjustment, attitude control, and rotation (Huang *et al.* 2011; Kozubskii *et al.* 2003; Mazouffre 2016). However, Hall thruster plumes consist of electrons, ions, neutrals and sputters, which can lead to surface contamination and surface charging of the spacecraft (Goebel *et al.* 2014; Tajmar *et al.* 2001). Therefore, with the continuous expansion of in-orbit application missions, the influence of the thruster plume on spacecraft operation has received more attention. Meanwhile, the interactions between the thruster plume and the spacecraft determine the layout of the thruster and other spacecraft carrying equipment, such as the solar arrays, antennas, and so on. Additionally, the plume density and distribution also determine the working parameters of the thruster, such as plume divergence angle and thrust density. That is, the higher the axial plume density, the smaller the plume divergence angle, and the higher the thrust density. As shown in Fig. 1, the 12.5 kW Hall thruster with a (discharge channel) diameter of 200 mm is developed by the Lanzhou Institute of Physics (LIP), and its application is for the future nuclear power propulsion and deep space exploration in China. To optimize the working parameters of the 12.5 kW Hall thruster, it is necessary to study the plume characteristics of the thruster.

Received: Oct. 14, 2024 | **Accepted:** Feb. 04, 2025
Peer Review History: Single Blind Peer Review.
Section editor: José A. Fritz F. Rocco

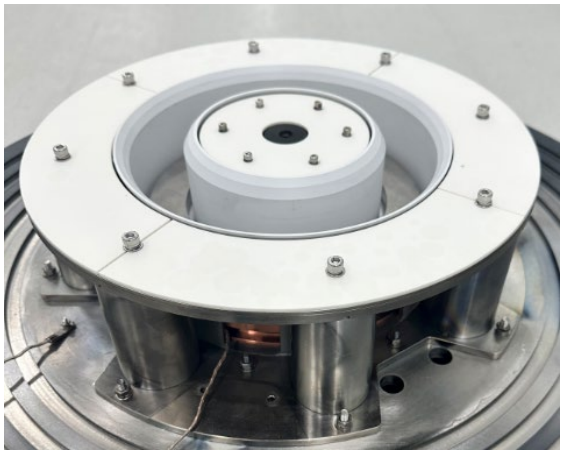

Source: Elaborated by the authors.

Figure 1. The 12.5 kW Hall thruster developed by LIP.

The study of plume characteristics includes simulation and experimental measurement. There are three methods to simulate the plume characteristics: the fluid method, the full particle method, and the hybrid simulation. The difference between the three methods is the treatment of particles in the plume, that is, the use of fluid equations, particle motion equations, or a combination of the two types of equations to deal with the plume particles. Since the 1980s, some researchers have calculated and studied the plume of Hall thrusters. Typically, David *et al.* (1999) built a plume simulation model of a Hall thruster using the particle-in-cell-direct Monte Carlo collision (PIC-DSMC) method, and the results indicated that the plume consists of quasi-neutral plasma and collision-free electrons, hence the effect of the magnetic field (MF) on the thruster plume can be ignored. Additionally, the simulation results of beam current density were in good agreement with the experimental results. Taccogna *et al.* (2008) investigated collisions between different types of particles in the plume by the full particle simulation method. In the simulation, the electron temperature in the plume near-field region was assumed to be constant, and the plume as a whole was electrically neutral. Boyd *et al.* (2002) and Keidar *et al.* (2005) added a fluid model to the full particle model, which was used to solve electron density. The simulations were compared with the measurement results, and the results showed that plasma density in the near-field of the plume was close to the measurements. Since 2010, studies on plume modeling of Hall thrusters have gradually increased, and the models were mainly based on axial and radial modeling, while the solution area included the discharge channel and near-field plume region. For example, Andreussi *et al.* (2017) and Kawashima *et al.* (2018) used a two-dimensional (z and r direction) hybrid model to simulate the Hall thruster discharge channel and plume near-field region, and the solution of potential in the evaluation was treated as plasma quasi-neutral, that is, the effect of self-consistent electric field (ES) was ignored, and the experiments showed that it had no great influence on the simulation results of the discharge process. Domínguez *et al.* (2018) and Campanell *et al.* (2015) established a full-particle radial model of the discharge channel by using the PIC-MCC method, and concluded that the non-Maxwell distribution of electrons in the discharge channel has some influence on the plasma sheath. Therefore, controlling the secondary electron emission coefficient can keep the stability of the sheath. Merino *et al.* (2015) used a full fluid model to quickly predict the spatial distribution of plasma in the plume near-field region and found that the fluid method can greatly expand the calculation region, and the boundary conditions (including thruster input parameters, plume boundary settings, etc.) have an important impact on the simulation results of the thruster plume. Cao *et al.* (2020), Lu *et al.* (2018), and other researchers have carried out computational simulations on the charge exchange (CEX) ion distribution and etching of discharge channels. The measurements of plume characteristics include contact methods and non-contact method represented by probe measurement (Long *et al.* 2024) (such as Faraday probe, Langmuir probe) and optical measurements (Linnell *et al.* 2006) (such as laser-induced fluorescence method, spectral diagnosis). Measuring the plume current density with probes is the cheapest and easiest to achieve, while optical measurement requires expensive instruments and a special transparent glass for the vacuum chamber to obtain the plume parameters. As mentioned above, although there have been many simulation and measurement studies on the plume characteristics of Hall thrusters, there are few studies on the plume characteristics of high-power Hall thrusters, and most of research chooses full-particle or hybrid simulation models, which

require high cost and time to develop models. Moreover, due to the urgent on-orbit tasks, the development cycle of thrusters is correspondingly shortened, and the final structure of thrusters often needs several iterations of design improvement. Therefore, developing an efficient, cheap, and accurate plume simulation model and obtaining the characteristics of the plume have obvious engineering value for accelerating the structural improvement of high-power Hall thrusters.

The purpose of this paper is to quickly establish an efficient and cheap plume model using commercial software, and the model needs to have a certain level of precision. The plume characteristics are then evaluated, and the simulations are verified by experiments. According to the comparison results, the accuracy of the model will be verified, and it will be estimated whether the model can be used for rapid simulation of plume characteristics. Additionally, theoretical results can be used for the possible improvement of existing structures improvement in the future.

METHODOLOGY

As shown in Fig. 1, the 12.5 kW Hall thruster adopts a centering cathode design, where the cathode is installed at the center of the thruster's geometric symmetry. This facilitates the symmetry of the plume and results in higher anode efficiency. Considering the advantages of the three plume simulation methods and the purpose of rapid iterative thruster structure optimization, the fluid method is adopted to obtain the plume characteristics. Therefore, COMSOL Multiphysics coupling software is used for the simulation, hence COMSOL is suitable for inexpensive and quick fluid parameter studies, but the convergence of calculations needs to be solved (Gabriel 2005).

The fluid method is to obtain the relevant parameters of the plume particles by solving the magneto-fluid equation, with certain assumptions made in the calculation, which mainly include:

- All three types of particles (electrons, ions, and atoms) in the plume are simulated using fluid equations;
- The calculation area consists of the discharge channel and the plume near-filed region (2 to 3 times the diameter of the discharge channel (Andreussi *et al.* 2017), but considering the comparison with the test, the length of calculation area is extended to 1 m;
- The ES in the plume area is an electrostatic field, and the ES distribution is obtained by the potential relationship when the thruster is working steadily. Here, the influence of the plasma self-consistent ES is ignored, as the plasma beam in the Hall thruster plume region is electrically neutral due to the relatively weak MF;
- The influence of the cathode on the plume is ignored. This is because, after the discharge is stabilized, the number of the electrons emitted from the hollow cathode is constant. Therefore, an electron flux boundary is set in the fluid model to simulate the electron emission. Additionally, the cathode has no effect on the distribution of the MF in the plume diffusion region, and the potential of the cathode is only about 11 to 18 V relative to the power ground, which is much lower than the potential difference (600 V) between the anode and the power ground;
- The influence of the plasma sheath on the potential distribution is ignored. This is because, to satisfy the quasi-neutrality of the plasma, the mesh size used in the fluid model is much larger than the Debye length of the plasma (about 0.2 to 1 mm) in the plume region.

As shown in Figs. 1 and 2, the 12.5 kW Hall thruster adopts an axisymmetric structure design, with the cathode is mounted at the geometric center of the thruster. This is because the built-in cathode can obtain a smaller plume divergence angle, and can effectively improve the anode efficiency (Ding *et al.* 2018; Hofer *et al.* 2008). Figure 2a shows the installation relationship of various components inside the thruster, with the magnetic pole being the main supporting component. Other components (such as the anode, discharge channel, etc.) are installed on the magnetic pole. In this structural design, the thermal conduction path can be divided into axial (along the discharge channel) and radial (along the diffusion plate). The axial heat conduction path is mainly "the energy deposition in the discharge channel – interior stay and magnetic pole – diffusion plate and thruster base." The components along this path are mainly metal, and the heat transfer is mainly through contact heat conduction. In contrast, due to the gaps between the various components in the radial direction, most of the heat is transferred in the form of surface-to-surface radiation, with some heat transferred along the diffusion plate. Therefore, although the thruster operates at a power of up to 12.5 kW , the high-temperature components are mainly the discharge channel and the interior coil (measured temperature ranges from 300 to 318 °C), while the exterior coil and the base have lower temperatures (ranging from 150 to 210 °C).

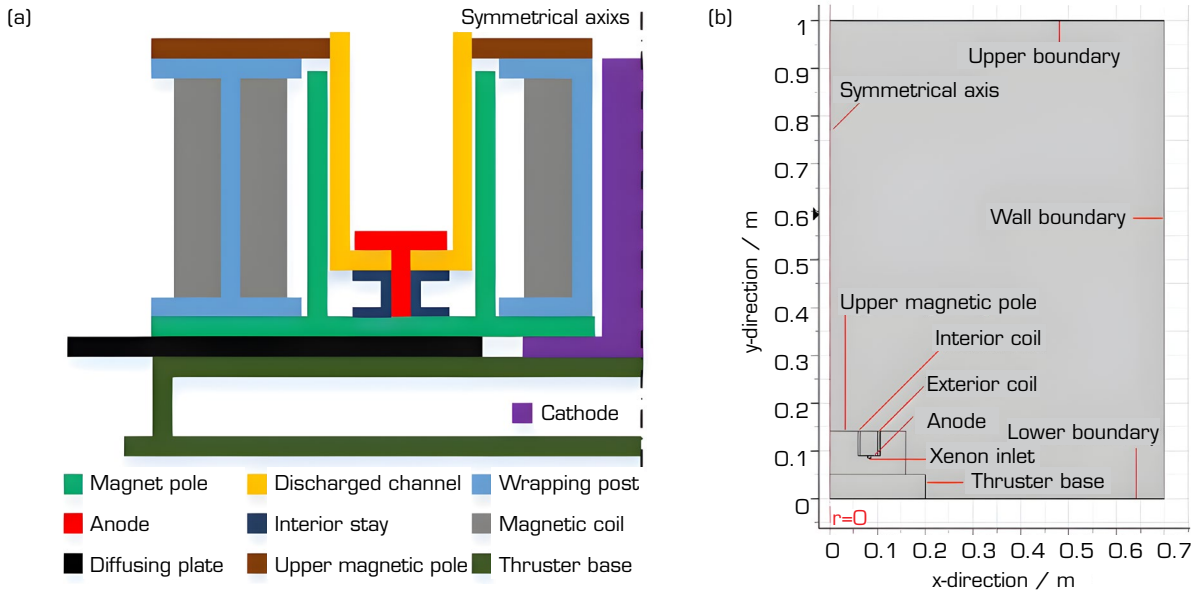

Source: Elaborated by the authors.

Figure 2. Structure and simulation area of 12.5 kW Hall thruster. (a) Internal structure of the thruster; (b) Schematic diagram of simulation area.

Figure 2b shows a schematic diagram of the simulation area. The discharge area is axisymmetric and includes both the thruster and the plume diffusion area. The thruster model is built according to the real structure size, but only the discharge channel, coil, magnetic pole, and base are retained to simulate the discharge process. The radius of the upper magnetic pole and the width and depth of the discharge channel are 0.16 m, 0.03 m and 0.06 m, respectively. Additionally, the plume diffusion area includes the upper and lower boundaries as well as the wall boundary. The upper boundary simulates the moving plane of the Faraday probe. According to the actual position of the probe when the plume is measured, the distances between the upper and lower boundaries, as well as between the upper boundary and the thruster outlet, are set to 1 m to 0.86 m, respectively. The lower boundary simulates the thruster-mounting platform. According to the distance between the vacuum facility wall and the thruster, the distance between the wall boundary and the symmetrical axis is set to be 0.7 m, ensuring that the plume can be fully diffused.

Table 1 shows the rated parameters of the 12.5 kW Hall thruster. The electrical parameters and gas supply parameters listed in the table, such as anode voltage and current, and flow rate of the cathode and the anode, are determined after several iterations of performance tests in a vacuum environment. The thrust is measured by the pressure sensor for several times and obtained by averaging. Other parameters, such as specific impulse and efficiency, are obtained through theoretical calculation. Additionally, it is noted that the voltages of the anode, keeper, and base are all the difference relative to the power ground.

Table 1. Rated work parameters of a 12.5 kW Hall thruster.

Parameters	Values	Parameters	Values
Thrust/mN	533	Efficiency	52.9%
Specific impulse/s	2,800	Total power/W	12,500
Anode voltage/V	600	Anode flow rate/mgs^{-1}	20
Anode current/A	20.4	Cathode flow rate/mgs^{-1}	0.47
Keeper voltage/V	18	Base voltage/V	25
Turns of interior coil	490	Turns of exterior coil	260
Interior coil current/A	5	Exterior coil current/A	3

Source: Elaborated by the authors.

Discharge model and boundary settings

As shown in Fig. 2b, the discharge model retains the main discharge area according to its real size, and the discharge channel is integrated with the plume diffusion region, so that the simulation results are continuous. According to the discharge process of the thruster, the static ES module, MF module, single-phase flow (SPF) module, and drift-diffusion (DD) module of COMSOL are used in the simulation. The ES, the MF, and the SPF modules are used to obtain the distribution of the ES, MF, as well as the fluid velocity, neutral density, and other parameters. These parameters are used as calculation boundaries or setting conditions for the DD module.

The ES distribution directly affects the motion of ions and electrons, thereby changing the plume characteristics and significantly affecting the diffusion of the plume. As shown in Fig. 2 and Table 1, the potentials of the upper magnetic pole and the base are equal, set to 25 V. The potential of the upper boundary, as shown in Fig. 2b, is set to -30 V because the upper boundary simulates the moving plane of the probe. That is, the bias voltage applied on the probe is -30 V, with the negative of the bias power is grounded to the vacuum facility. Moreover, the potentials of the wall boundary and the lower boundary, as shown in Fig. 2b, are set to 0 V to simulate the facility wall. The ES can be calculated by $E = -\nabla V$. Additionally, the ES distribution is obtained based on the assumption that the plasma beam is electrically neutral, and the self-consistent electric field of the discharged plasma is ignored.

The MF distribution mainly affects the movement of electrons, which indirectly influences the movement of ions and changes the plume distribution. According to previous research, adjusting the MF distribution has noticeable effects on the plume divergence angle and ion density in the plume near-field region (Yu *et al.* 2017). As shown in Fig. 2b and Table 1, the coil closer to the symmetrical axis is the interior coil, and the turns and current of the interior coil are set to 490 and 5 A, respectively, while those of the exterior coil are set to 260 and 3 A, respectively.

In the neutral fluid simulation of the calculation area, the boundaries are first set according to the actual size and gas supply rate, and then the boundaries are slightly adjusted according to whether the result is convergent. As shown in Fig. 2b and Table 1, for the discharge channel, the interior diameter of the xenon inlet is 5 mm. The SPF module is adopted to obtain the velocity and pressure of the neutral gas in the calculation area. According to the previous temperature measurement results of the 12.5 kW Hall thruster, the temperature of the inner wrapping post and the discharge channel after stable operation is in the range of 300-318 °C. In many cases, Hall thrusters operate under a low-density neutral gas, so the Knudsen number of the neutral gas is much greater than one, while collisions between the neutrals can be ignored and the neutrals in the channel are free-molecule (Katz *et al.* 2011). In the simulation, the turbulence is ignored, and the boundaries of all walls in the channel are set to no-slip, meaning that the velocity of the fluid on the walls is zero. The xenon inlet is set to a mass flow boundary with a value of 20 mg·s^{-1}, and the flow direction is from the inlet to the channel. The initial pressure of the calculation region is set to 0.005 Pa, and the upper, wall, and lower boundaries shown in Fig. 2b are set as gas outlets with a pressure of 0.008 Pa (measured vacuum degree after stable operation).

Based on the DD equation, the DD module is used to simulate the generation and diffusion of the charged plasma in the calculation area, which regards the plasma as a fluid flow, and the flow is effected by magnetic and ES. The DD module mainly contains the electron continuity equation, the electron DD equation, and the energy balance equation. The electron continuity equation is expressed as follows:

$$\frac{\partial n_e}{\partial t} + \nabla \Gamma_e = R_e \tag{1}$$

where n_e is the plasma density, Γ_e is the electron flux in the channel, and R_e is the generation rate of the electrons (unit is m^{-3}s^{-1}). The electrons are produced by elastic, excitation, and ionizing collisions, respectively, and the reaction rate coefficients corresponding to different collision type are defined as k_1, k_2, and k_3. Each collision type has its own reaction coefficient (Miller *et al.* 2002), and all the reaction coefficients have a similar expression, which is expressed as $\langle \sigma v \rangle$, where σ and v are the collision cross section and the total collision frequency (determined by the electron temperature T_e), respectively. It is noted that elastic collisions are ignored, as there are almost no Maxwellian electrons produced during elastic collisions, but only energy transfer occurs in most cases. Therefore, the excitation reaction rate r_2 and the ionization reaction rate r_3 are expressed as $k_2 n_0 n_e$ and $k_3 n_0 n_e$. The production of Maxwellian electrons and the total reaction rate R_e in discharge channel can be expressed as:

$$\begin{aligned} e + X_e^* &\rightarrow X_e^+ + 2e \\ e + X_e &\rightarrow X_e^+ + 2e \\ R_e &= r_2 + r_3 = k_2 n_0 n_e + k_3 n_0 n_e \end{aligned} \tag{2}$$

The electron flux Γ_e is obtained by the DD equation, which is shown as:

$$\Gamma_e = -(\mu_e \cdot E) n_e - D_e \cdot \nabla n_e \tag{3}$$

where E and μ_e are the ES and electron migration coefficient, respectively, and μ_e can be expressed as:

$$\mu_e = e / m_e \nu (1 + \Omega_e^2) \tag{4}$$

Considering that the number of electrons generated by collisions between ions and ions, ions and atoms, is much lower than that generated by collisions between electrons and atoms, electrons and ions. Therefore, collisions between ions and ions and between ions and atoms are ignored. Thus, the total collision frequency ν is consisted of the collision frequency ν_{en} between electrons and neutral atoms, as well as the collision frequency ν_{ei} between electrons and ions. ν_{en} and ν_{ei} are given by Katz *et al.* (2004) and Book (1987), respectively. Ω_e is the term of electron Hall parameter correction and reflects the ability of the MF to restrain the electrons, which can be expressed as $\Omega_e = eB/m_e\nu$, where B is MF distribution. D_e is the electron diffusion coefficient, which has Einstein's relation with μ_e, and expressed as $D_e = \mu_e T_e$. The energy balance equation can be expressed as:

$$\frac{\partial n_\varepsilon}{\partial t} + \nabla \Gamma_\varepsilon + \mathbf{E} \cdot \Gamma_e = S_{en} \tag{5}$$

where n_ε and Γ_ε are the energy density and energy density flux of the electrons, respectively, and determined by μ_e, n_e and T_e. S_{en} is the collision energy loss, consisting of the elastic collision energy loss d_{e1}, the first-order energy loss d_{e2} and the second-order energy loss d_{e3} caused by the ionizing collision between electrons and atoms. Table 2 gives the setting of the main parameters, where k is Boltzmann constant and m_e is electron mass.

Table 2. Main parameter settings in DD module.

Parameters	Expressions	Description
k_1	$1.99^{-14}\ T_e^{0.93}\ e^{-0.41/Te}$	Elastic collision coefficient
k_2	$1.93^{-19}\ e^{-11.6/Te}/T_e^{0.5}[8eT_e/\pi/m_e]^{0.5}]$	Exciting collision coefficient
k_3	$10^{-20}(3.97 + 0.643T_e - 0.0368T_e^2) \times e^{-12.127/Te}$ $(8eT_e/\pi/m_e)^{0.5}$	Ionizing collision coefficient
r_1	$k_1\ n_0\ n_e$	Elastic reaction rate
r_2	$k_2\ n_0\ n_e$	Exciting reaction rate
r_3	$k_3\ n_0\ n_e$	Ionizing reaction rate
$d_{e1}; d_{e2}; d_{e2}$	0; 8.31; 12.13	Energy loss
R_e	$r_2 + r_3$	Production rate of electrons
S_{en}	$-e(r_1\ d_{e1} + r_2\ d_{e2} + r_3\ d_{e3})$	Collision energy loss
σ_{en}	$6.6^{-19}\ (T_e/4 - 0.1)/[1+(T_e/4)^{1.6}]$	Collision cross section
$\ln\Lambda$	$23^{-0.5} \log\ (10^{-6}\ n_e/T_e^3)$	Coulomb logarithm
V_{en}	$\sigma_{en}\ n_0\ (8kT_e/\pi/m_e)^{0.5}$	Collision frequency (electrons and neutrals)
V_{ei}	$2.9^{-12}\ n_e\ ln\Lambda/T_e^{1.5}$	Collision frequency (electrons and ions)
μ_e	$e/[m_e\ (\nu_{en} + \nu_{ei})]$	Migration coefficient

Source: Elaborated by the authors.

The initial density and energy of the electrons in the entire model are set as 1×10^{18} m^{-3} and 3 eV, respectively. As shown in Fig. 2b, the reaction rate R_e is only set in the channel, so the plume mainly diffuses by the effect of electric and MFs. The electron reflection coefficient of the discharge channel walls, shown in Fig. 2b, is set to 0, meaning that the secondary electrons emission by the wall is ignored. Additionally, since the distance between the upper and the wall boundaries from the discharge channel is 0.86 m and 0.7 m, respectively, which is much larger than the characteristic length of the thruster (i.e., the width of discharge channel of 0.03 m), it can be approximatively considered that the distance between the upper and the wall boundary from the thruster is infinite, and the electron flux at these two boundaries is set to 0, that is, the density and energy of electrons are both 0. After defining all the boundaries and parameters of the model, then the simulation processes in the MF, ES, and SPF modules are set to steady-state simulations. Moreover, the simulation process in the DD module is set as a transient simulation, and the simulation duration is from 10^{-8} s to 10^{-1} s, during which the discharge process and plume diffusion can reach a steady state.

Simulation results and analysis

The potential distribution and MF distribution are shown in Figs. 3a and b. Figure 3a shows that the closer to the outlet of the thruster, the higher the potential and the larger the potential gradient. Additionally, the distribution of potential shows obvious axisymmetric characteristics and the direction of ion motion is perpendicular to the isopotential line. Therefore, the plume extracted from the discharge channel is divergent, and the divergence angle has a strong relationship with the curvature of the isopotential line.

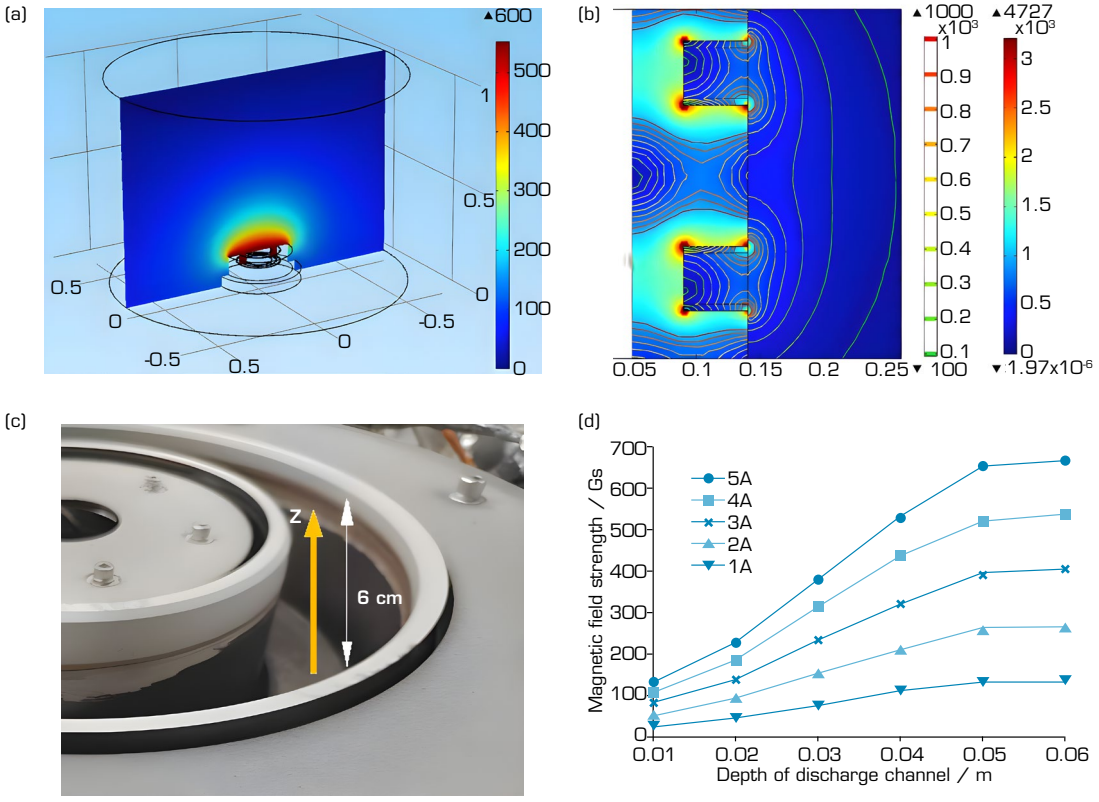

Source: Elaborated by the authors.

Figure 3. Potential and MF distribution and MF measurement. (a) Potential/V; (b) MF distribution/Gs; (c) MF test; (d) Measured MF/Gs.

Based on the interior and exterior coil turns and current conditions in Table 1 (the turns and current of the interior and exterior coil are 490/5 A and 260/3 A, respectively), Fig. 3b shows the MF distribution in the channel and plume near-field region. The MF has no effect on ion motion, while it mainly restrains electron motion and controls the ionization reaction rate. The distribution of isopotential lines indicates that the MF in the channel is not uniform, and there is an obvious gradient along the axis of the discharge channel. This is because the MF is generated by the coil, and the number of turns and current of the interior coil are greater than those of the exterior

coil, so the closer to the interior coil of the channel, the stronger the MF. Meanwhile, the MF closer to the channel bottom is lower, which means the discharge process will mainly occur in the upper part of the discharge channel. According to the previous research (Morozov *et al.* 2000), most discharge processes of the Hall thruster are concentrated in the upper 30% region of the discharge channel.

To estimate the accuracy of the simulation results, a LakeShore Model-425 Gauss meter is used to measure the MF in the channel, and the test method is shown in Fig. 3c. Along the centerline of the discharge channel with a depth of 6 cm, that is, along the z-axis in the positive direction shown in the figure, the MF at different points is measured with a step size of 1 cm. Additionally, the same current is applied to the interior and exterior coils, ranging from 1 A to 5 A, and the MF is measured five times in steps of 1 A. The measurement results are shown in Fig. 3d. According to the same conditions as the test, the MF at the same measuring points for different currents is calculated, and the comparison results are shown in Table 3. Table 3 shows that the comparison errors are all less than 5%, which proves that the simulation results are accurate.

Table 3. Comparison of simulation and measurement results of MF.

Current/ A	5	4	3	2	1
Measurements/Gs	668.20	536.83	402.54	267.78	134.23
Simulations/Gs	650.1	539.4	404.7	272.5	135.3
Errors	2.71%	0.48%	0.53%	1.78%	0.79%

Source: Elaborated by the authors.

The fluid velocity simulation results in the calculation area are shown in Fig. 4a, and it can be concluded that the fluid velocity is highest along the axis of the discharge channel, with the average value is in the range of 160 to 200 ms^{-1}. Meanwhile, the fluid ejecting into the plume region shows an obvious diffusion characteristic. In the calculation, it is found that the inner friction of the fluid should be ignored to better achieve computational convergence. Additionally, it is further found that the backflow of the fluid should be ignored to achieve convergence. The neutral density is shown in Fig. 4b. The result shows that the neutral density in the channel is the highest, and in most areas of the channel, the neutral density is in the range of 2×10^{19} to 3×10^{19} m^{-3}. The calculation results can be verified by equation 6, where P is the average pressure in the channel, $\bar{v}$ is the average velocity of xenon atoms, and r_1 and r_2 are the inner circle radius and outer circle radius of the discharge channel, respectively. The average velocity of xenon atoms can be obtained by the gas temperature, then the average pressure in the discharge channel is calculated to be about 0.12 Pa, thus the average atom density in the channel is about 2.9×10^{19} m^{-3}, which is basically consistent with the simulations. Moreover, the simulations are consistent with the previous calculation results (Katz *et al.* 2011), which show that the atom density in the channel is in the range of 1×10^{19} to 5×10^{19} m^{-3}.

$$P = m_a \bar{v} / \pi (r_2^2 - r_1^2) \tag{6}$$

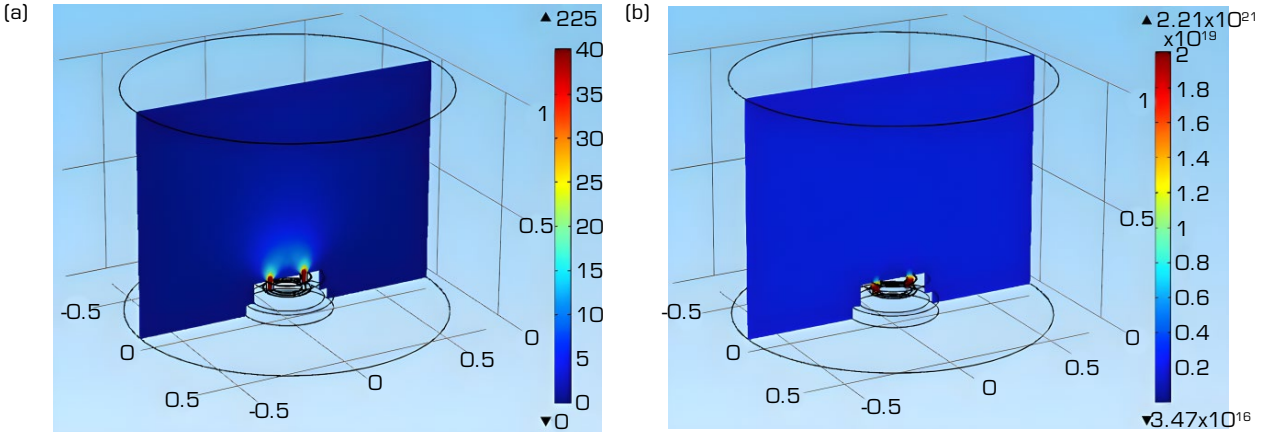

Source: Elaborated by the authors.

Figure 4. Distribution of fluid velocity and neutral density. (a) Fluid velocity/ms^{-1}; (b) Neutral density/m^{-3}.

Figures 5a and d show the characteristics of the discharge plasma in the channel and the plume region. As shown in Fig. 5a, the plasma density along the centerline of the channel is the highest, and the plasma density decreases less along the axial direction. However, the plasma density decreases rapidly along the radial direction of the plume calculation region. This is mainly due to the distribution of the potential isopotential lines, and the ions move in a direction perpendicular to the equipotential line. As shown in Fig. 3a, the decay of potential in the axial direction is low, so the ions move rapidly along the axis under the acceleration of the ES, and the reduction in plasma density is not significant. However, the radial potential distribution decays obviously and has little effect on charged particles. Therefore, the motion of ions along the radial direction is mainly diffusion, and the plasma density decreases rapidly. According to Figs. 5a and b, the plasma density and the electron temperature from the discharge channel outlet to the upper boundary of the plume region are in the range of 6.2×10^{16} to 5.2×10^{17} m^{-3} and 1.8 to 12.2 eV, respectively, while the plasma density and the electron temperature from the channel outlet to the wall boundary are in the range of 4.6×10^{9} to 5.2×10^{17} m^{-3} and 1.2 to 12.8 eV. The distribution of electron temperature shown in Fig. 5b expresses a similar characteristic to the potential distribution. This is because the acceleration of ions is determined by the isopotential lines and the electric potential in the channel and the plume near field area is the highest, thus the ions in these regions can obtain the highest acceleration energy.

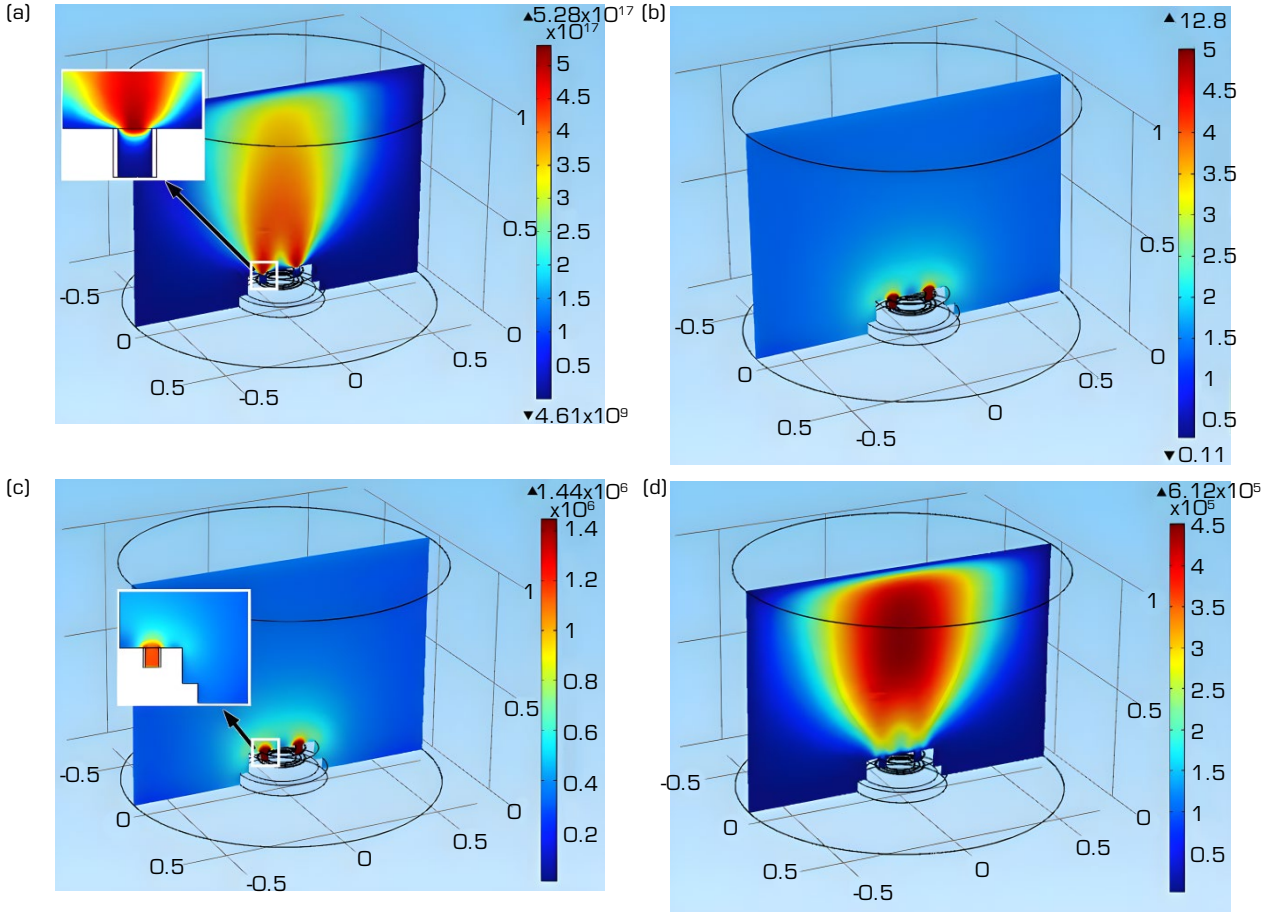

Source: Elaborated by the authors.

Figure 5. Characteristics of thruster plume. (a) Plasma density/m^{-3}; (b) Electron temperature/eV; (c) Electron-neutral collision frequency/Hz; (d) Electron-ion collision frequency/Hz.

Figures 5c and d show the collision frequencies of electrons and neutrals and electrons and ions, respectively. Collision between electrons and neutrals shows the main ionization and ion production region, while the latter shows the divalent ion production region. The higher the density of divalent ions, the higher the thrust loss of the thruster will be, and the higher

density of the divalent ions will lead to the enhancement of discharge energy loss and the decrease in discharge efficiency, causing higher erosion to the discharge channel. As shown in the figure, the collision frequency between electrons and neutrals is in the range of 1×10^6 to 1.44×10^6 Hz, and which is almost concentrated in the channel, where the atomic density is highest. The collision frequency between electrons and ions is in the range of 1.5×10^5 to 4.5×10^5 Hz and is concentrated in the plume diffusion region.

Test results and comparison

Figure 6a shows the simulated plume density near the upper boundary, with the plume density is in the range of 4.9×10^{13} to 8.4×10^{15} m^{-3}. To estimate the precision of the simulation results, a plume test of the 12.5 kW Hall thruster is carried out. The test is conducted in a large vacuum facility at LIP, the vacuum chamber having a diameter of 8 m and a length of 16 m, and the facility is equipped with 6 external cryogenic pumps and 30 internal cryogenic pumps, which can maintain a vacuum of 1.7×10^{-3} Pa under the rated working conditions of the thruster. As shown in Figs. 6b and c, the plume test uses a moving single Faraday probe to collect the beam current. The diameter of the probe collector is 8 mm, and the length of the stainless steel sleeve outside the probe is 14 mm. The thruster is mounted on a fixed bracket, the Faraday probe is installed on a travel mechanism, and the distance from the probe to the thruster base is 0.9 m (z-axis shown in Fig. 6c), and both are at the same height (the height in the y-axis is 0.6 m). The scanning range of the probe is 0 to 1.2 m, and the thruster is installed in the middle position of the scanning distance, that is, at a location of 0.6 m on the x-axis. However, in the actual test, only a distance of 0 mm to 0.8 m is scanned, as the beam has a symmetrical distribution, so the measurement is stopped after scanning the beam peak.

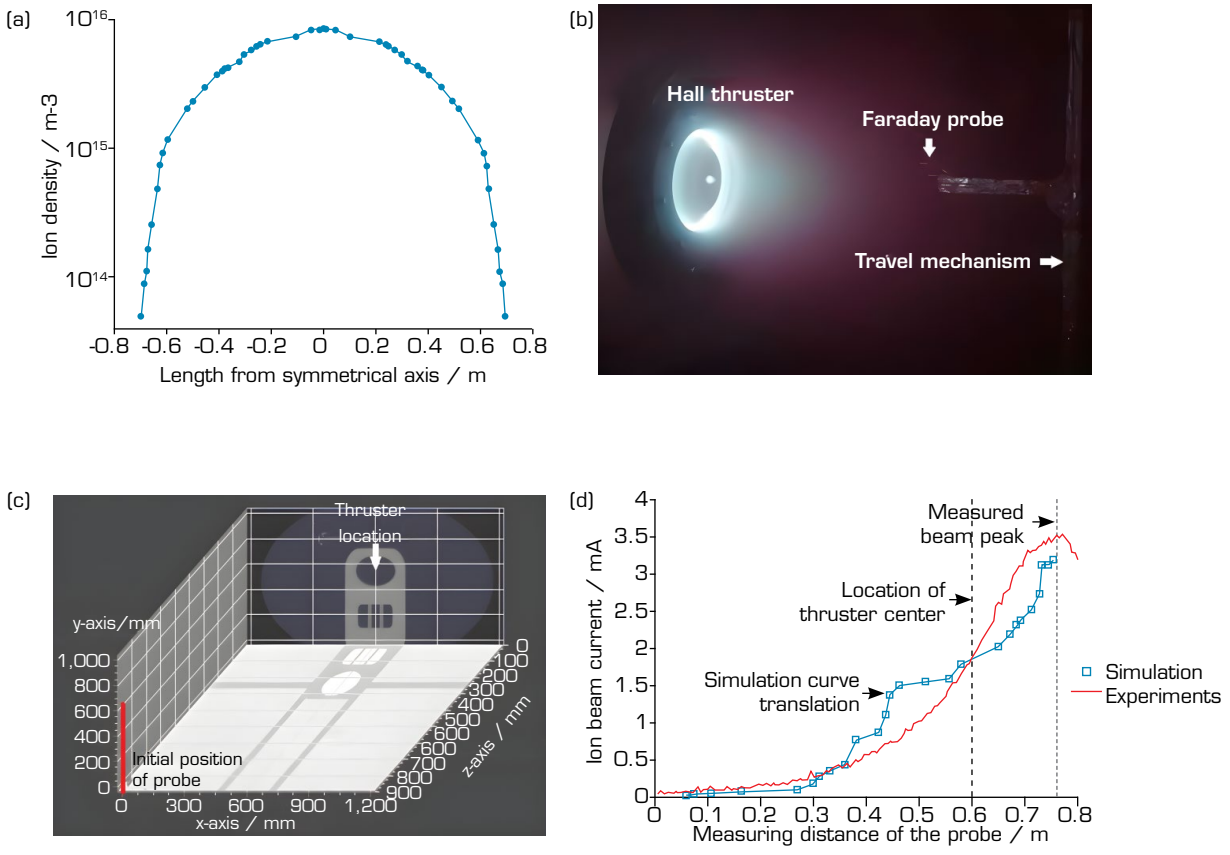

Source: Elaborated by the authors.

Figure 6. Plume measurement and the results comparison. (a) Plume density on the upper boundary/m^{-3}; (b) Plume measurement; (c) Location of the thruster and probe; (d) Comparison of results.

Since the Faraday probe collects beam current, then the simulated plasma density shown in Fig. 6a should be converted into current, as shown in Eq. 7,

$$I_{\mathrm{b}} = n_{\mathrm{e}} e v_{\mathrm{i}} \pi r_0^2 \tag{7}$$

where I_b is the ion beam, v_i and r_0 are the ion velocity (which is calculated to be 2.96×10^4 ms^{-1}) and the radius of the probe collection surface (which is 4 mm), respectively. According to Eq. 7, the plasma density shown in Fig. 6a is converted into beam current to compare with the measurements, and the comparison results are shown in Fig. 6d. It should be noted that the beam peak does not appear at the projection of the thruster center on the moving plane of the probe, that is, 600 mm, but at 780 mm. Therefore, to compare with the test, the simulation curve is translated to ensure that the beam peak also appears at 780 mm. The beam peak does not appear in the projection of the thruster center mainly because the centerline of the thruster is not perpendicular to the moving plane of the probe during installation, and even a small angular deviation will cause a large displacement of the projection of the centerline on the moving plane. Additionally, the focusing effect of the MF on plasma and the uneven gas supply in the discharge channel will lead to the deviation of the beam peak.

According to the comparison results, the simulation results are consistent with the experimental results. However, near the edge of the plume, that is, where the probe moves from 0.3 m to 0.5 m, the variation of the beam current obtained by simulation is obviously higher than that of the measured results (changes from 0.29 A to 1.01 A). This is because the simulated plasma density changes from 1.11×10^{15} to 6.15×10^{15} in this measurement distance (-0.48 m to -0.28 m shown in Fig. 6a), and the corresponding beam current changes from 0.25 A to 1.50 A. Similarly, within the probe travel distance of 0.6 m to 0.78 m, the simulated plasma density changes from 6.78×10^{15} to 8.05×10^{15} in a distance of -0.18 m to 0 m (as shown in Fig. 6a), and the simulated beam current is lower than the measured value. In conclusion, the measured beam current changes more gradually, while the simulations show that the variation of beam current is greater near the edge of the plume, and the closer to the beam center, the smaller the change in beam current, which is due to the boundary settings in the simulation, especially the distribution of ES s and MF s. Additionally, the defects of the fluid method are also an important source of error. Although there are some errors between simulations and measurements in some test distances, in general, the variation of simulated beam current coincides well with the variation trend of measured results.

CONCLUSION

The plume characteristics are of great significance for the on-orbit application and design optimization of the thruster. Therefore, an efficient and inexpensive plume model based on COMSOL software is established and verified by beam current measurement. The comparison results of simulations and experiments show that the fluid method can rapidly obtain plume characteristics, and the fluid method is suitable for the study of macroscopic parameters of the thruster. The simulation model achieves the purpose of obtaining the plume characteristic parameters with certain accuracy, low cost, and rapidly execution. Moreover, the model has obvious engineering value in the optimization and improvement of Hall thruster. For example, according to the plume characteristics reflected in the model, the focus of the thruster plume can be evaluated. That is, based on simulated plume density, the divergence angle of the plume can be obtained, and then the MF and the ES can be constantly adjusted by the model to reduce the divergence angle as much as possible. However, the defects of the fluid method must be considered. Compared with the PIC method, the fluid method ignores the microscopic processes such as electron motion, the sheath in the discharge area, the collision between the particles, and the secondary electron emission effect on the wall of the channel, which will lead to a higher electron temperature of the plasma near the sheath, and a lower plasma density in the plume near-field region, resulting in errors with the measurements. Additionally, another defect of the fluid method is that it requires sufficient parameter settings in the calculation, which is an important source of error. Therefore, more tests and measurements should be conducted in the subsequent study to optimize the boundary and parameter settings of the model to minimize the errors.

CONFLICT OF INTEREST

Nothing to declare.

AUTHORS' CONTRIBUTION

Conceptualization: Sun M; **Methodology:** Sun M; **Software:** Sun M; **Validation:** Sun M and Liu C; **Formal analysis:** Sun M and Liu C; **Investigation:** Geng H and Gao J; **Resources:** Sun M and Li P; **Data Curation:** Sun M and Wang S; **Writing - Original Draft:** Sun M; **Writing - Review & Editing:** Sun M and Liu C; **Visualization:** - **Supervision:** Sun M; **Final approval:** Sun M.

DATA AVAILABILITY STATEMENT

The data are available in a data repository.

FUNDING

Not applicable.

ACKNOWLEDGMENTS

Not applicable.

REFERENCES

Andreussi T, Giannetti V, Leporini A, Saravia M, Andrenucci M (2017) Influence of the magnetic field configuration on the plasma flow in Hall thrusters. Plasma Phys Control Fusion 60(1):014015. https://doi.org/10.1088/1361-6587/aa8c4d

Book D (1987) NRL plasma formulary. Washington D.C.: Naval Research Laboratory.

Boyd D, Dressler A (2002) Far field modeling of the plasma plume of a Hall thruster. J Appl Phys 92(4):1764-1774. https://doi.org/10.1063/1.1492014

Campanell D, Wang H, Kaganovich D, Khrabrov V (2015) Self-amplification of electrons emitted from surfaces in plasmas with E×B fields. Plasma Sources Sci Technol 24(3):034010. https://doi.org/10.1088/0963-0252/24/3/034010

Cao XF, Liu H, Yu DR (2020) Research of the influence of the additional electrode on the Hall thruster plume by particle-in-cell simulation. Chin Phy. B 29(9):095204. https://doi.org/10.1088/1674-1056/aba2e3

David O, Daniel E, Colleen M, James M, Alec D (1999) Modeling of stationary plasma thruster-100 thruster plumes and implications for satellite design. J Propuls Power 15(2):345-357. https://doi.org/10.2514/2.5432

Ding Y, Li H, Li P, Jia B, Wei L, Su H, Sun H, Wang L, Yu D (2018) Effect of relative position between cathode and magnetic separatrix on the discharge characteristic of Hall thrusters. Vacuum 154:167-173. https://doi.org/10.1016/j.vacuum.2018.05.005

Dominguez-Vazquez A, Taccogna F, Ahedo E (2018) Particle modeling of radial electron dynamics in a controlled discharge of a Hall thruster. Plasma Sources Sci Technol 27(6):064006. https://doi.org/10.1088/1361-6595/aac968

Gabriel S (2005) COMSOL modelling of hollow cathodes. Paper presented 2005 35th International Electric Propulsion Conference Exhibit. Georgia Institute of Technology; Atlanta, USA.

Goebel D, Hofer R, Mikellides G, Katz I, Polk J, Dotson B (2014) Conducting wall Hall thrusters. IEEE Trans Plasma Sci 43(1):118-126. https://doi.org/10.1109/TPS.2014.2321110

Hofer R, Johnson K, Goebel D, Wirz R (2008) Effects of internally mounted cathodes on Hall thruster plume properties. IEEE Trans Plasma Sci 36(5):2004-2014. https://doi.org/10.1109/TPS.2008.2000962

Huang W, Gallimore D, Hofer R (2011) Neutral flow evolution in a six-kilowatt Hall thruster. J Propuls Power 27(3):553-563. https://doi.org/10.2514/1.B34048

Katz I, Mikellides I (2011) Neutral gas free molecular flow algorithm including ionization and walls for use in plasma simulations. J Comput Phys 230:1454-1464. https://doi.org/10.1016/j.jcp.2010.11.013

Katz I, Mikellides I, Goebel D (2004) Model of the plasma potential distribution in the plume of a hollow cathode. Paper presented 2004 40th Joint Propulsion Conference & Exhibit. AIAA; Ft. Lauderdale, USA.

Kawashima R, Hara K, Komurasaki K (2018) Numerical analysis of azimuthal rotating spokes in a crossed-field discharge plasma. Plasma Sources Sci Technol 27(3):035010. https://doi.org/10.1088/1361-6595/aab39c

Keidar M, Boyd D (2005) On the magnetic mirror effect in Hall thrusters. Appl Phys Lett 87(12):121501. https://doi.org/10.1063/1.2053351

Kozubskii N, Murashko M, Rylov P, Trifonov V, Khodnenko V, Kim V, Popov G, Obukhov VA (2003) Stationary plasma thrusters operate in space. Plasma Phys Rep 29(3):251-266. https://doi.org/10.1134/1.1561120

Linnell A, Gallimore D (2006) Internal plasma potential measurements of a Hall thruster using plasma lens focusing. Phys Plasmas 13(10):103504. https://doi.org/10.1063/1.2358331

Long J, Huang D, Sun M, Cheng Y, Wang J, Xu L, Guo N, Yang W (2024) Experimental study on beam characteristics of μHT-1 thruster under operating conditions adjustment. Vacuum 219:112735. https://doi.org/10.1016/j.vacuum.2023.112735

Lu C, Qiu P, Cao Y, Zhang T, Chen J (2018) A 3D particle model for the plume CEX simulation. Aeronaut J 122(1255):1425-1441. https://doi.org/10.1017/aer.2018.79

Mazouffre S (2016) Electric Propulsion for Satellites and Spacecraft: Established Technologies and Novel Approaches. Plasma Sources Sci Technol 25(3):033002. https://doi.org/10.1088/0963-0252/25/3/033002

Merino M, Cichocki F, Ahedo E (2015) A collisionless plasma thruster plume expansion model. Plasma Sources Sci Technol 24(3):035006. https://doi.org/10.1088/0963-0252/24/3/035006

Miller J, Pullins S, Levandier D, Chiu Y, Dressler R (2002) Xenon charge exchange cross sections for electrostatic thruster models. J Appl Phys 91(3):984-991. https://doi.org/10.1063/1.1426246

Morozov I, Savelev V (2000) One-dimensional hydrodynamic model of the atom and ion dynamics in a stationary plasma thruster. Plasma Phys Rep 26(3):219-224. https://doi.org/10.1134/1.952841

Taccogna F, Longo S, Capitelli M, Schneider R (2008) Surface-driven asymmetry and instability in the acceleration region of Hall thruster. Contrib Plasma Phys 48(4):375-386. https://doi.org/10.1002/ctpp.200810061

Tajmar M, Gonzalez J, Hilgers A (2001) Modeling of spacecraft-environment interactions on SMART-1. J Spacecr Rockets 38(3):393-399. https://doi.org/10.2514/2.3697

Yu D, Meng T, Ning Z, Liu H (2017) Confinement effect of cylindrical-separatrix-type magnetic field on the plume of magnetic focusing type Hall thruster. Plasma Sources Sci Technol 26(4):04LT02. https://doi.org/10.1088/1361-6595/aa6425